Designing Inflatable Structures

Mélina Skouras[1,2] Bernhard Thomaszewski[2] Peter Kaufmann[2] Akash Garg[3] Bernd Bickel [2]
Eitan Grinspun [3] Markus Gross[1,2]

[1]ETH Zurich [2]Disney Research Zurich [3]Columbia University

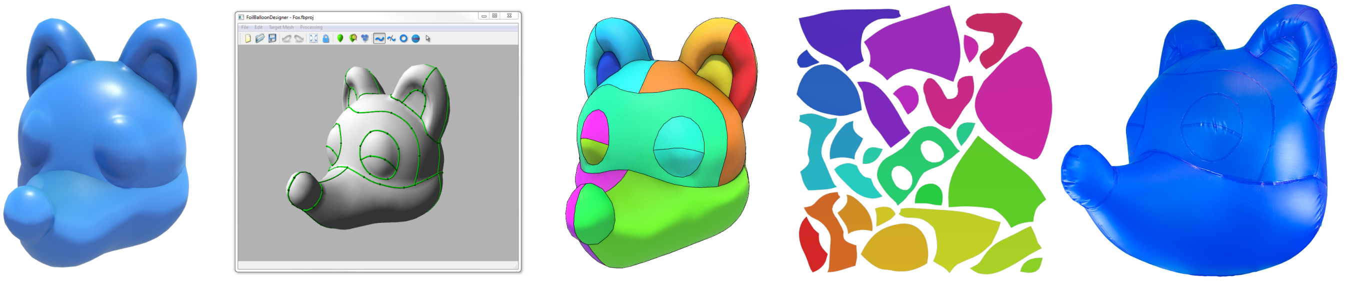

Figure 1: *We present an interactive design system that allows non-expert users to quickly create inflatable structures such as foil balloons, decorative items, or parade floats.*

Abstract

We propose an interactive, optimization-in-the-loop tool for designing inflatable structures. Given a target shape, the user draws a network of seams defining desired segment boundaries in 3D. Our method computes optimally-shaped flat panels for the segments, such that the inflated structure is as close as possible to the target while satisfying the desired seam positions. Our approach is underpinned by physics-based pattern optimization, accurate coarse-scale simulation using tension field theory, and a specialized constraint-optimization method. Our system is fast enough to warrant interactive exploration of different seam layouts, including internal connections, and their effects on the inflated shape. We demonstrate the resulting design process on a varied set of simulation examples, some of which we have fabricated, demonstrating excellent agreement with the design intent.

CR Categories: I.3.5 [Computer Graphics]: Computational Geometry and Object Modeling—Physically based modeling

Keywords:

Links: DL PDF

1 Introduction

Inflatables are structures made of flat membrane elements that assume complex curved shapes when pressurized. Thanks to their lightweight nature, rapid deployment, and cost efficiency, they enjoy widespread popularity in entertainment, advertisement, engineering, and architecture. From foil balloons to parade floats, inflatable furniture to portable architectural structures—myriad applications abound.

Designing inflatable structures requires solving a complicated *patterning* problem: what is the shape of the flat panels that we must cut, and how must we interconnect the panels, such that the final assembly inflates to the desired curved shape? This task is extremely challenging since the designer must anticipate, and invert, the effects of pressure on the shape of the structure, while simultaneously taking into account the aesthetics of seams. The combination of functional and aesthetic requirements make patterning the most difficult aspect of current manual design processes.

We propose a computational approach for the interactive design of inflatable structures. We assume that the designer already has a certain *target shape* at hand, perhaps acquired from real world data, designed via modeling software, or provided as a specification by a client. Our goal is to help the designer to make plans for an inflatable structure that corresponds to the given target.

Our approach ensures that the designer retains full control over aesthetic considerations; to do so, we lay aside fully automated approaches in favor of an interactive, optimization-in-the-loop methodology. As the designer sketches the proposed placement of seams, the underlying optimizer alleviates the iterative and error-prone tasks of reverse-engineering the physics of inflation, proposing a set of panels that best accommodate the desired seams and target shape.

The simplicity of this user experience requires some complex machinery under the hood. We develop a fast physics-based model for inflatable membranes motivated by tension field theory, and we employ a dedicated optimization method for computing the shape of the 2D patterns. We demonstrate the resulting design process on a set of inflatable structures with complex shapes and elaborate seam layouts. Finally, we validate the feasibility of our designs on three physical prototypes.

2 Related Work

Fabrication-Oriented Computational Design seeks to develop software, typically based on a mix of interaction- and optimization-based approaches, that facilitates the design of artifacts, taking into account not only considerations of functionality and aesthetics, but also manufacturing and assembly. Recently, several approaches have been presented for translating functional goals such as appearance [**?**], articulation [**?**; **?**], deformation behavior [Bickel et al. 2012; Skouras et al. 2013], kinematic motion [**?**; Coros et al. 2013; **?**], or a combination of these [**?**] to manufacturable parts. Stava et al. [2012] analyze 3D models and improve their structural strength for 3D printing. Usually interactivity is an essential component for keeping the designer in control of form-finding, allowing for example to explore physically valid furniture designs [Umetani et al. 2012; Lau et al. 2011] or designing garments [Umetani et al. 2011].

Computation of optimal 2D patterns has been investigated by Wang and Tang [**?**] in the context of compression garment design. While their system aims at producing clothing with prescribed strains and normal pressures and uses tensile truss bars, our tool focuses on matching an inflated shape and relies on a continuum-based energy formulation.

Interactive tools for designing plush toys, *Pillow* and *Plushie*, were proposed by Mori and Igarshi [2007; **?**]. The workflow of our system draws inspiration from *Pillow*'s. However, unlike our system, *Pillow* employs flattening that does not include an inflation-based metric nor warrants satisfaction of fabrication constraints. As for *Plushie*, extended to non-stretchy materials by Futura et al. [2010], it is a modeling tool which is complemented by our work: whereas *Plushie* projects begin with a blank canvas, our projects begin with a given target shape. *Plushie* helps the user to focus on the modeling task, whereas our work helps the user to focus on the control of seam placement and panel shape. The latter point of view is essential for obtaining compelling designs for myriad organic forms, and for geometric shapes such as simple sphere (see Fig. **??**).

Most recently, Skouras et al. [2012] presented a computational tool for design of rubber balloons. Rubber balloons (a) stretch significantly during inflation, (b) have 3D rest shapes fabricated by dipping a mold into liquid rubber, and (c) are typically pliant even when maximally inflated. By contrast, our inflatable structures (a) have great membrane stiffness and negligible stretching strain, yield more durable artifacts; (b) are manufactured by assembly of piecewise *flat* rest shapes, facilitating maintenance and repair, allowing for larger physical dimensions, and permitting decoration with paint, ink, or other appliques using standard printing methods; and (c) can be quite stiff when inflated, expanding the potential functionality beyond the realm of purely decorative. Finally, the space of designs we consider is richer than that spanned by rubber balloons, including complex shapes with sharp creases.

Automatic Segmentation and Parametrization techniques seek to create mappings with low distortion [Hormann et al. 2007]. For example, *DCharts* [Julius et al. 2005] segments models into almost developable patches, which can then be flattened using *ABF++* [Sheffer et al. 2005] to create approximately conformal parametrizations with small stretch. Flattening multiple panels independently generally produces incompatible seam lengths, requiring alterations such as pleats or cuts that complicate fabrication and impose a very particular visual appearance. To address this point, Wang [2008] considered flattening subject to both minimal stretch and seam length compatibility. We draw inspiration from Wang's approach to compute initial guesses for pattern optimization.

An alternative approach is to approximate a 3D shape by a set of ruled surfaces such as cones and planes [Shatz et al. 2006], generalized cylinders [Massarwi et al. 2007]), or paper strips [Mitani and Suzuki 2004]. Also, there are a number of tools for modeling developable surfaces. Kilian et al. [2008] use curved creases to design complex-shaped surfaces from planar sheets. Solomon et al. [2012] describe an interactive design system that exactly satisfies discrete developability conditions at all times. While these methods work well for designing physically-realizable surfaces, e.g. made out of paper, developability does not guarantee that the object's surface is in equilibrium under pressure. In our case, we are optimizing for developable (flat) patches, that, when stitched together and then inflated, resemble a 3D shape at a desired equilibrium. However, our fast physics-based simulation approach does not necessarily compute an *inflated surface* with zero Gaussian curvature and therefore does not guarantee a piecewise developable surface.

Cloth and Shell Simulation Similar to inflatables, cloth buckles at the onset of compression. This behavior leads to the characteristic folding patterns that define the typical appearance of real textiles, but it is inherently difficult to treat numerically: compression gives rise to negative eigenvalues in the force Jacobian and thus slows or even breaks most linear solvers. Choi and Ko [2002] proposed a mass-spring model that turns off force and Jacobian contribution from compressed springs and replaces them with custom-tailored *buckling springs*. Another approach to combat indefiniteness was presented by Teran et al. [2005], who clamp negative eigenvalues of elemental stiffness matrices. Instead of trying to avoid indefiniteness, the method of Rohmer et al. [2010] exploits the compression field extracted from elemental deformation tensors in order to add detailed wrinkles to a coarse simulation. Inspired by tension field theory [**?**; **?**], we propose a fast physics-based model that addresses the difficulty of wrinkling analysis based on a relaxed energy which fades to zero before compressive stresses can occur.

3 System Overview

The goal of our system is a workflow that makes the design of inflatable structures intuitive and efficient for the user. We start the description by making precise the notion of inflatable structures.

3.1 Anatomy of Inflatable Structures

Inflatable structures are made from flat *panels*, i.e., thin layers of metallic foil, vinyl, or textile. While our approach does not exclude stretchy materials such as rubber per se, we target structures that show little stretch but large bending deformations. We therefore focus on quasi-inextensible materials that exhibit a high resistance to stretching, but are compliant to bending.

A connection between two panels is called a *seam*. Depending on the type of material, seams are created through gluing, heat sealing, or stitching. As an important design constraints, the segments forming the seam should have the same length on both panels. Otherwise, the design must be altered during manufacturing using cuts or pleats.

The shape of inflatable structures is governed by the requirement that they have to be *stable under pressure*: the pressure forces must be balanced by membrane forces in every point on the surface. This equilibrium constraint puts limits on what kind of shapes can be obtained with a structure that consists of single closed surface. However, the space of possible designs can be significantly enlarged by allowing for *internal connections* (see Fig. **??**). Such internal connections can be used to attach parts of the surface to each other that would otherwise be pushed apart by the pressure forces. They can also be used to create creased feature curves.

3.2 Design Loop

Interface The design interface consists of three views: the inflate view, target view, and pattern view (see Figure **??**). Each new design session starts by loading a closed triangle mesh that represents the 3D target shape. The user incrementally builds a seam layout

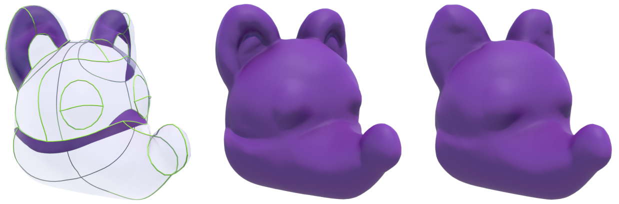

Figure 2: *Internal connections (left) allow the designer to realize shapes with sharp creases and concave features (middle) that would be poorly approximated without internal structures (right).*

that partitions the target mesh into a set of segments. Once a seam layout or edit is committed, our system flattens the corresponding segments and begins pattern optimization (Sec. **??**) in the background. The inflate view immediately shows a preliminary shape for the resulting inflated structure, obtained by inflating the model with the current patterns in simulation (Sec. **??**). Both views are continuously updated while the optimization proceeds in the background.

Seam Design The user draws seams directly on the target model using a spline tool that implements a *geodesics* metaphor, i.e., connects seam points by taking an approximately shortest path on the surface. We represent seam curves using cubic Hermite splines that are defined through a coarse set of 3D control points. For segmentation, we simply project the spline curve onto the surface mesh.The seam tool supports snap-on functionality in order to link new seams to existing ones. In addition, the user can also edit existing seams by simply dragging control points.

Generally, some of the seams will have aesthetic purposes or requirements, while others simply subdivide a larger region in order to increase the shape approximation quality. For each of the seams, the user can therefore specify a weight that indicates how important it is for the seam to remain in its original location with respect to the target shape. These conditions are then enforced through corresponding objectives during pattern optimization.

Internal Connections As a necessary condition for a given shape to be a feasible balloon, it has to be stable under pressure. Clearly, this requirement limits the space of shapes that can be realized as balloons. However, the design space can be significantly enlarged by allowing for internal connections, i.e., panels that are not visible from the outside and serve a purely functional purpose. Internal connections are created by connecting existing seams on the surface as indicated by the user. Technically, internal connections are no different from the other, visible patches. However, paired with our optimization, internal connections provide a powerful tool for creating complex shapes with distinct features (see Fig. **??**).

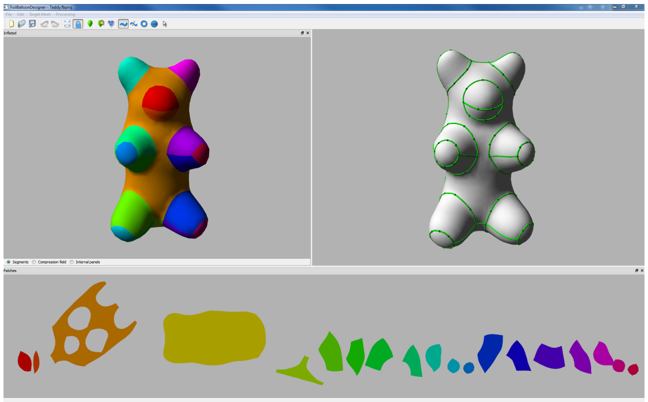

Figure 3: *Our design interface, showing the inflated view (top left), target view (top right), and pattern view (bottom).*

Pattern Optimization tightly integrates with simulation in order to compute flat panels that allow for an optimal approximation of the target shape. Whenever a seam layout or edit is committed by the user, the involved segments are first flattened in order to obtain an initial guess for the pattern shape (Sec. **??**). Afterwards, the shapes of the flat panels are computed by optimizing various objectives, including shape approximation and seam quality (Sec. **??**). In order to deal with the overall nonlinear nature of the problem and the large changes in pattern shapes, our system uses an iterative optimization algorithm based on Sequential Quadratic Programming (SQP) with integrated remeshing (Sec. **??**). Although this method can take some time to fully converge, the results are typically visually stable after a few seconds only. The user can thus quickly explore different seam layouts without disturbing delay.

4 Simulation

As a core component of our design system, we must be able to rapidly compute the deformed shape of inflatable structures. Like many other thin structures, inflatables exhibit a strong resistance to stretching but will wrinkle at the onset of compression. This behavior poses challenges that our simulation must confront efficiently.

4.1 Origins of Compression

As a didactic example, consider the simple foil balloon depicted in Fig. **??**, assembled from two disc-shaped panels. When inflating the balloon, we expect that (1) the distance between the centers of the two panels increases due to *pressure*; (2) the seam remains on its original plane due to *symmetry*; (3) each radial line, extending from the center to the seam, will remain unstretched due to *inextensibility*. To meet these requirements the diameter *must* decrease during inflation. Correspondingly, the circumference must shrink, implying a compressive deformation on the seam that is resolved through the typical wrinkles observed in foil balloons (Fig. **??**, *right*). Wrinkling is a characteristic trait of thin surface structures, but a major struggle for simulation codes. First, compressions give rise to negative eigenvalues in the energy Hessian, thus breaking the fundamental assumption of most fast linear solvers, i.e., a positive-definite matrix. Second, since the location of wrinkles can usually not be predicted, a simulation mesh with uniformly high resolution

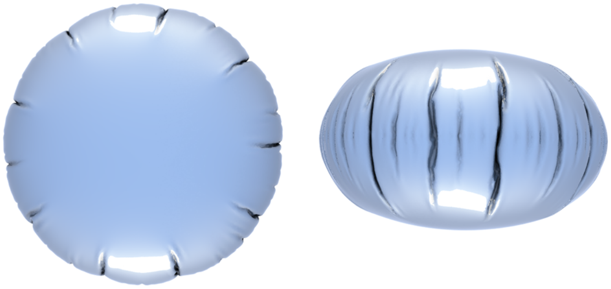

Figure 4: *Compression-induced wrinkling in a simple foil balloon.*

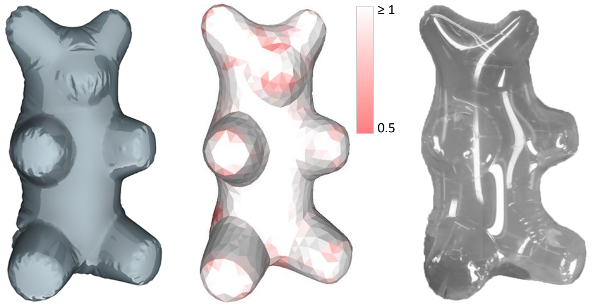

Figure 5: *Wrinkling analysis using the full model (*left*), compressive deformations from the tension field model (*middle*), real-world prototype (*right*). Colors indicate compressed elements with compression stretches ranging from $\lambda_2 = 0.5$ to $\lambda_2 = 1$.*

is required. Clearly, both these properties are highly detrimental to efficiency.

The problem of compressions in thin surfaces is not new to graphics. For example, Choi and Ko [2002] proposed a modified mass-spring system that allows for stable animations of buckling cloth. Both the original work and its extension to triangle meshes [**?**] handle compressions along buckling springs that connect pairs of particles that are at topological distance two. However, in order to provide accurate results even for coarse simulation meshes, we would like a model that is able to handle compressions along arbitrary directions, irrespective of mesh structure.

4.2 Tension Field Theory

The wrinkling of membranes has been intensively studied in mathematical and physical sciences [**?**; **?**]. The difficulty of wrinkling analysis stems from the fact that the elastic energy density is not convex in the presence of compressions, jeopardizing the uniqueness and existence of solutions. Tension field theory offers a solution to this problem by postulating a *relaxed* energy density that reflects the average energy value in wrinkled regions and gracefully fades to zero before compressive stresses can occur. The underlying reasoning is that while wrinkled regions can carry longitudinal loads (so called tension trajectories), they do not exhibit resistance to transversal deformations. This formulation enables a macroscopic treatment of wrinkling that accurately captures the deformation behavior on the coarse level but abstracts away geometric detail. There are two important advantages of this approach, both of which translate directly into computational efficiency: it requires fewer elements and it removes the problems due to indefiniteness. We will make this concept precise below. Using the tension field when optimizing for the panel shapes has the additional advantage of easing the distance measurement between simulated and target meshes, since wrinkles are homogenized by a smooth surface.

Although the tension field approach does not directly provide geometric information on the wrinkles, the compression field does give strong indications on the locations and the directions of the expected wrinkles. We found these regions to be in very good correspondence with both the locations predicted by a high-res simulation of the full model and our actual, fabricated prototypes.

Relaxed Energy Density The deformation around a given point on the surface is described by the deformation gradient $\mathbf{F}$. With a view to the relaxed strain energy density, we introduce the 2×2 right Cauchy Green tensor

$$\mathbf{C} = \mathbf{F}^T\mathbf{F} = \lambda_1\mathbf{N}_1\mathbf{N}_1^t + \lambda_2\mathbf{N}_2\mathbf{N}_2^t\,, \tag{1}$$

in terms of its principal stretches λ_1, λ_2 and corresponding eigenvectors $\mathbf{N}_1$, $\mathbf{N}_2$. Without loss of generality, we assume that $\lambda_1 \geq \lambda_2$. Following Skouras et al. [2012] and assuming that the material is incompressible and does not exhibit transverse shearing, we expand $\mathbf{C}$ to the 3×3 tensor

$$\hat{\mathbf{C}} = \begin{bmatrix} \mathbf{C} & 0 \\ 0 & J^{-1} \end{bmatrix}\,, \tag{2}$$

where $J = \lambda_1\lambda_2$ is the determinant of $\mathbf{C}$. We opt for a Neo-Hookean material, whose strain energy density is defined in terms of the first invariant of $\hat{\mathbf{C}}$, $I_1 = Tr(\hat{\mathbf{C}})$, by

$$\psi(I_1) = \kappa\,(I_1 - 3) = \kappa\left(\lambda_1 + \lambda_2 + \frac{1}{\lambda_1\lambda_2} - 3\right) = \psi(\lambda_1, \lambda_2)\,, \tag{3}$$

where κ is the stiffness coefficient. As described above, the essence of tension field theory can be condensed into a relaxed strain energy density

$$\tilde{\psi}(\lambda_1, \lambda_2) = \begin{cases} 0 & \lambda_1 < 1, \lambda_2 < 1 \\ \psi(\lambda_1, \tilde{\lambda}_2(\lambda_1)) & \lambda_1 \geq 1, \lambda_2 < \tilde{\lambda}_2(\lambda_1) \\ \psi(\lambda_1, \lambda_2) & \lambda_1 \geq 1, \lambda_2 \geq \tilde{\lambda}_2(\lambda_1) \end{cases}\,, \tag{4}$$

where $\tilde{\lambda}_2$ is the energetic minimum of λ_2,

$$\tilde{\lambda}_2(\lambda_1) = \underset{\lambda_2}{\text{argmin}}\ \psi(\lambda_1, \lambda_2) = \frac{1}{\sqrt{\lambda_1}}\,. \tag{5}$$

The three cases listed in (3) are illustrated in the inset figure. For the first case (a), the surface is assumed to be *slack*, i.e., both stretches are negative and the energy is set to zero. The second case (b) corresponds to wrinkling and the original model is applied with the compressive stretch replaced by its energetically optimal value. The third case (c) corresponds to a *taught* surface with both stretches positive for which the original model can be applied without modifications. Since the first and second cases are energetically optimal with respect to compressive stretch, the material model will never give rise to compressive stresses.

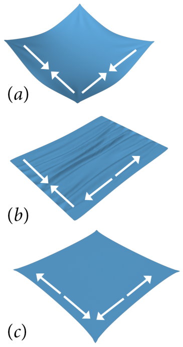

It is worth noting that the modified energy density $\tilde{\psi}$ is convex but only C^1 continuous. Although we did not notice any adverse effects when solving for equilibrium states, the discontinuous force derivatives pose a significant problem for optimization. We therefore smooth the transitions between the different regimes using quadratic interpolation, as described in the supplementary material.

4.3 Discretization

Notation Let m denote the number of external and internal panels of the inflatable structure. The geometry of each panel in its undeformed state is described by a triangle mesh $\mathcal{P}_i$. The deformed mesh, comprising all panels, is denoted by $\mathcal{M}$. Furthermore, we let $\mathbf{x} \in \mathbb{R}^{3n}$ denote the vector of deformed positions for the n nodes of the surface. Likewise, $\mathbf{X} \in \mathbb{R}^{2N}$ holds the positions of the N undeformed panel vertices in their two-dimensional domain. Note that vertices corresponding to panel boundaries are not duplicated in $\mathcal{M}$. Instead, we use a single set of coordinates to describe their common deformed positions.

Forces We use a standard finite element approach based on Constant Strain Triangles for discretizing (3) and its derivatives. The internal forces $\mathbf{f}_i^{\text{int}}$ at each node are obtained as

$$\mathbf{f}_i^{\text{int}} = -\sum_{e \in \mathcal{F}_i} \frac{\partial \tilde{\psi}^e}{\partial \mathbf{x}_i} V_e = -\sum_{e \in \mathcal{F}_i} \left(\frac{\partial \tilde{\psi}^e}{\partial \lambda_1^e} \frac{\partial \lambda_i^e}{\partial \mathbf{x}_i} + \frac{\partial \tilde{\psi}^e}{\partial \lambda_2^e} \frac{\partial \lambda_2^e}{\partial \mathbf{x}_i} \right) h A_e \ ,$$

where $\mathcal{F}_i$ denotes the set of triangle elements incident to the vertex i, A_e is the initial area of element e, h is the thickness of the panels and $V_e = hA_e$ is the volume of e. It is evident from this expression that the gradient and Hessian of (3) require the first and second derivatives of the principal stretches. We provide the corresponding derivations and other details in a supplemental document.

The pressure forces are defined directly in the discrete setting as

$$\mathbf{f}_i^{\text{p}} = p \frac{\partial V}{\partial \mathbf{x}_i} = \sum_{e \in \mathcal{F}_i} \frac{1}{3} p A_e \mathbf{n}_e \ , \tag{6}$$

where p is the pressure value and $\mathbf{n}_e$ and A_e are the outward normal and the area of element e. The shape of the inflated structure can then be computed by solving the static equilibrium problem

$$\mathbf{f}_i^{\text{int}}(\mathbf{x}, \mathbf{X}) + \mathbf{f}_i^{\text{p}}(\mathbf{x}) = 0, \ 1 \leq i \leq n \ . \tag{7}$$

5 Automatic Pattern Generation

Our system combines user-guided seam design with automatic pattern generation. During seam design, the user will repeatedly invoke the pattern optimization scheme in order to explore the effect of a given layout or edit on the inflated structure.

Formally, given a target mesh $\mathcal{T}$ and a set of seam lines segmenting the mesh into m parts, we seek to find optimal panel shapes $\mathbf{X}$ for each part such that the distance between the inflated mesh $\mathcal{M}$ and the target mesh $\mathcal{T}$ is as small as possible. We cast this goal into the form of a constrained minimization problem,

$$\min_{\mathbf{x}, \mathbf{X}} E(\mathbf{x}, \mathbf{X}) \quad \text{s.t. } \mathbf{f}(\mathbf{x}, \mathbf{X}) = \mathbf{0} \ , \tag{8}$$

where the constraints $\mathbf{f}(\mathbf{x}, \mathbf{X}) = \mathbf{0}$ require force equilibrium in every node and $E(\mathbf{x}, \mathbf{X})$ summarizes various objective terms. We solve this optimization problem using the Sequential Quadratic Programming (SQP) method described by Byrd et al. [**?**], which guarantees progress even in non-convex regions.

5.1 Objectives

Distance to Target In order to quantify the distance between the inflated mesh $\mathcal{M}$ and the target mesh $\mathcal{T}$, we construct a distance field on $\mathcal{T}$ using implicit moving least squares [**?**]. The distance penalty is defined as

$$E_{\text{target}}(\mathbf{x}) = \sum_i \frac{\sum_k \mathbf{n}_k \cdot (\mathbf{x}_i - \mathbf{c}_k) \phi_k(\mathbf{x})}{\sum_k \phi_k(\mathbf{x})} \ , \tag{9}$$

where $\phi_k(\mathbf{x}) = \left(1 - \frac{||\mathbf{x} - \mathbf{X}_k||_2^2}{h^2}\right)^4$ are locally-supported kernel functions that vanish beyond their support radius h, that we set to twice the average length of the target mesh edges, while $\mathbf{c}_k$ and $\mathbf{n}_k$ denote the vertex positions and normals of $\mathcal{T}$, respectively. This measure allows the vertices of $\mathcal{M}$ to slide freely over $\mathcal{T}$, whereas a simpler pair-wise vertex distance would lead to bias and thus unnecessarily restrict approximation quality.

Seam Locations Seams are critical to the aesthetics of inflatable structures. Our interface provides tools that allow the user to rapidly create seam layouts on the target surface. Some of these seams simply split larger areas into smaller parts, in which case their exact location is not critical. Our optimization can leverage such freedom for better shape approximation. Others, however, serve an important aesthetic role that the final inflatable structure has to respect by adhering to the shape and location of the seams. We therefore let the user specify the importance of a given seam $\mathcal{S}_i$ by assigning a weight σ_i to it that determines how strongly the corresponding seam vertices on $\mathcal{M}$ are attracted to their target locations on $\mathcal{S}_i$. We define the penalty function based on vertex-wise L_2-distance as

$$E_{\text{seam}}^i(\mathbf{x}) = \sigma_i \sum_{j \in \mathcal{S}_j} ||\mathbf{x}_j - \mathbf{s}_j||_2^2 \ , \tag{10}$$

where $\mathbf{s}_j$ denotes the target position for $\mathbf{x}_j$ on the seam. It is worth noting that the seam vertices are not restricted to be a subset of the vertices of $\mathcal{M}$—seams can run freely across the target surface.

Fabrication Constraints In order for two panels $\mathcal{P}_j$ and $\mathcal{P}_k$ to join in a seam, the corresponding boundary segments must have the same length on both panels. Otherwise, discrepancies have to be corrected *a posteriori* using cuts or pleats, which increases fabrication time and degrades the visual quality of the product. We enforce this equal-length requirement per seam as

$$E_{\text{length}}(\mathbf{X}) = \sum_{i=1}^{s_e} (L_j^i(\mathbf{X}) - L_k^i(\mathbf{X}))^2 \ , \tag{11}$$

where s_e is the number of seam edges in $\mathcal{M}$ and L_j^i and L_k^i are the lengths of corresponding edge vectors on the boundaries of $\mathcal{P}_j$ and $\mathcal{P}_k$. While the lengths of the boundary segments have to be the same, they can, and generally will, exhibit different curvatures. Nevertheless, boundaries should still remain smooth, which we encourage with a corresponding penalty term,

$$E_{\text{smooth}}(\mathbf{X}) = \sum_{i=1}^{m} \sum_{j=1}^{b_i} ||\mathbf{Q}_l^i - 2\mathbf{Q}_j^i + \mathbf{Q}_r^i||_2^2 \ , \tag{12}$$

where b_i is the number of non-corner boundary vertices $\mathbf{Q}^i$ of panel $\mathcal{P}_i$, whereas $\mathbf{Q}_l^i$ and $\mathbf{Q}_r^i$ denote the left and right neighbors of boundary vertex $\mathbf{Q}_j^i$.

Regularization The distance energy (**??**) allows the vertices $\mathbf{x}$ to slide on the target surface, but this freedom comes at the price of a nullspace: for any displacement of a given internal panel vertex $\mathbf{X}_i$, there is a corresponding world-space displacement $\mathbf{x}_i$ such that neither objectives nor constraints change. In order to obtain a well-posed problem, we use a Laplacian regularizer that asks for a smooth distribution of internal panel vertices as

$$E_{\text{laplace}}(\mathbf{X}) = \sum_{i=1}^{m} \sum_{j=1}^{n_i} \mathcal{L}(\mathbf{X}_j) \ , \tag{13}$$

where $\mathcal{L}(\mathbf{X}_j)$ is the Tutte Laplacian [**?**]. As a desirable side effect, this regularizer also promotes well-shaped elements.

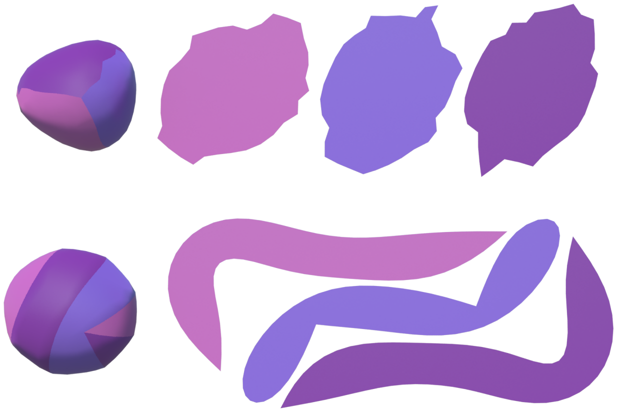

Figure 6: *Pattern optimization for a spherical balloon. The balloon (left) and its patterns (right) are shown for the initial guess (top), and after optimization (bottom).*

5.2 Initial Flattening

The final shape of the patterns is obtained by solving the constrained minimization problem (11). However, a good initial guess is crucial for rapid convergence. In principle, any mesh parametrization method can be used to create an initial guess. A particular aspect of our setting is, however, that the shape of the panels is entirely defined by their boundary vertices—the shape of interior elements is, to a large extent, an afterthought. Among the many existing methods, we therefore took inspiration in one that preserves the lengths of the segment boundaries [Wang 2008].

We start by converting the user-provided seams, represented by smooth spline curves, into sets of edge vectors, defining a segmentation of the target mesh $\mathcal{T}$. For each segment, we first flatten its boundary $\mathbf{q}^i$ by minimizing an objective function that penalizes squared differences in edge lengths and internal angles as

$$E_{\text{fl}}(\mathbf{Q}^i) = \sum_{j=1}^{b_i} \tfrac{1}{l_{ij}}(L_{ij}(\mathbf{Q}^i) - l_{ij})^2 + l_j(\Theta_j(\mathbf{Q}^i) - \theta_j)^2 \ , \quad (14)$$

where L_{ij} are the lengths of the boundary edges of panel $\mathcal{P}_i$ and l_{ij} are the corresponding lengths in $\mathcal{T}$. Moreover, Θ_j is the sum of internal angles around $\mathbf{Q}^i_j$, θ_j is the corresponding quantity on $\mathcal{T}$, and l_j is the average length of the two edges incident to $\mathbf{q}^i_j$. The resulting nonlinear problem is solved with a few iterations of Newton's method. Keeping the boundary vertices fixed, the positions of the internal vertices are then computed by minimizing a Laplacian energy analogous to (**??**), which amounts to a single linear solve.

We note that, although a good initial guess helps speed convergence, our optimization scheme is not very sensitive to this choice. The example shown in Fig. **??** puts this robustness to a test, using *D-Charts* and *ABF++* (see [Julius et al. 2005]) as initial guess for the three panels of a spherical balloon. Here, the lengths of the panel boundaries are very different from the corresponding lengths on the target shape. Nevertheless, our method is able to find panel shapes that allow for a close approximation of the target. It is also worth noting that, since the seams were not restricted to stay in place, the final patterns are very different from the initial guess, revealing a surprisingly symmetric and elegant solution.

5.3 Remeshing

Fig. **??** exemplifies the potential difference between initial and final patterns. In order to robustly handle such extreme changes in size and shape, we integrate the optimization with a remeshing method that maintains well-shaped elements at all times. A number of works in graphics have explored the integration of remeshing and simulation, either globally [O'Brien and Hodgins 1999; Bargteil et al. 2007; Wojtan and Turk 2008] or in a locally adaptive manner [Wicke et al. 2010; Narain et al. 2012]. Since our mesh sizes are comparatively small, we opt for a global remeshing scheme that builds on *Triangle* [**?**]. Remeshing is invoked whenever the aspect ratio of an element falls below a given threshold. We first resample the boundaries of the patches to satisfy a minimum- and maximum-length criteria on the edges, maintaining correspondence between adjacent patches. We then invoke *Triangle* to remesh the interior of each patch and carbon-copy all changes to the inflated mesh as well as the target mesh.

6 Results

We used our design system to create a diverse set of inflatable structures, seven of which we present and discuss in this section. For validation, we also created physical prototypes for three of these examples. The design interface and the results are demonstrated in detail in the accompanying video and in Figure **??** and Figure **??**. The fabricated models are made out of PVC plastic sheets. The optimized patches generated by our system were cut with a computer-controlled cutting machine and then manually hot sealed. In the following section, we validate some of our design decisions and discuss our results in more detail.

Simulation We compared our relaxed energy density based on tension field theory to a full simulation using the strain energy density of an incompressible Neo-Hookean material as stated in Equation 2. The full simulation for the Teddy model shown in Figure **??** with ≈59k elements took more than two hours, whereas our relaxed energy density is computationally more efficient because it requires fewer elements and avoids problems due to indefiniteness. We tested our simulation approach with several different resolutions, ranging from ≈3k elements to ≈59k elements, and report the approximation error in Figure **??**. The computation for the three meshes of ≈3k, ≈15k and ≈59k elements took 4.5, 77 and 157 seconds, respectively. In practice, we observed that already with a coarse mesh we are able to obtain satisfactory accuracy. Although the relaxed energy formulation comes at the cost of not exhibiting any wrinkles in the simulated geometry, areas where wrinkling oc-

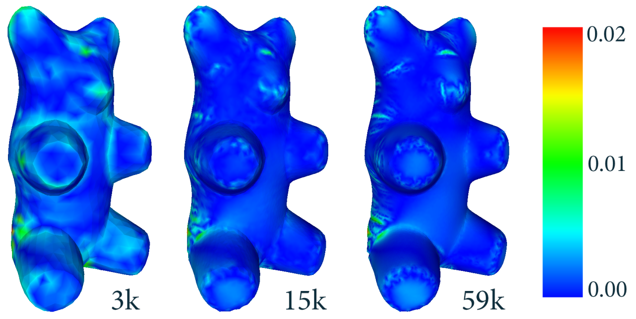

Figure 7: *Comparison of simulations with relaxed energy model on meshes with resolutions of 3k, 15k, and 59k elements to a reference simulation using the original energy on the 59k mesh. Colors indicate per-vertex difference for a unit size model.*

curs can be inferred from the compression field. By displaying this information as a color-coded overlay, we can provide the user with feedback on wrinkle location and amplitude during seam design.

Performance of Optimization To evaluate the performance of our optimization, we start from a given seam layout and measure the required time for convergence, when no later edit is performed. This comprises the initial flattening, initialization of all data structures, remeshing operations and subsequent data structures updates, and optimization itself. The optimization is the most expensive step of the process but the evaluation of the different involved quantities largely dominates the linear solves. All computations were done on a standard desktop computer with 3.20 GHz and 12 cores. Our research prototype is written in C++ and, except of solving the system of equations, not yet parallelized, leaving room for significant speed-ups. As a stopping criterion, we require the infinity-norm of the gradient of the Lagrangian corresponding to (11) to be smaller than $\text{tol} = 10^{-3}$, whereas a tighter tolerance of $\text{tol} = 10^{-5}$ is used for the forces. We use the same thresholds for all models presented in this paper. Table **??** lists detailed performance numbers of our algorithm for all examples, including the number of elements, the number of required remeshing steps, and the number of SQP iterations. In practice, we observed that already after a few iterations the result is close to the final solution. We therefore opted to visualize the incremental steps of the optimization to the user, providing fast visual feedback and intuition about the quality of the seam placement. As shown in Table **??**, after less than a minute, the relative error measured between the starting point of the optimization and the final converged result is below 5%, and therefore provides sufficient accuracy for a pre-visualization.

Seam Placement The approximation quality, i.e., how well a given inflatable structure matches its target shape, depends on the number of patches as well as the seam layout. In our experiments we observed that there is a tradeoff between shape approximation and aesthetic requirements. As illustrated in Figure **??**, seams can slide significantly during the optimization on the target surface. We allow the user to intuitively control the admissible amount of sliding by adjusting the weight of the corresponding penalty term (Equation **??**). If seams are assigned a small weight, they can move such as to optimize the overall shape approximation. If seams are assigned a high weight, they stay close to their target location in 3D. As the location of the seams is generally very important for the aesthetics of the inflatable structure, we used relatively high weights for all models, except for the "Sphere". This approach proved particularly important and effective for modeling the "Fox" (Figure **??**), for which characteristic features such as the eyes, and eyelids were delineated by corresponding seams.

Our interface allows non-expert users to efficiently add, edit, and replace seams and explore the impact of these operations on the inflated shape in an interactive manner. A demonstration of the design process can be found in the accompanying video. On average, designing a foil balloon took between 8 minutes for simple models ("Teddy") and less than half an hour for sophisticated models with internal connections ("Fox").

Internal Connections Several of our models ("Fox", "Elephant", "Flower", "Twisty") rely on internal connections, which are created by connecting existing seams on the surface as indicated by the user. As shown in Figure **??**, internal connections can be used, for example, to create sharp concave creases—a salient feature for many models. Figure **??** and Figure **??** visualize the internal patches generated by our method and demonstrate that the resulting inflated shapes are in very good agreement with the desired behavior.

7 Limitations and Future Work

We have presented a design system for creating inflatable structures made from flat panels. The enabling technology of our system is an automatic physics-based pattern generation method, combining fast simulation based on tension field theory and robust constraint optimization. Combined with an intuitive user interface, even non-expert users are able to design and explore intricate structures by simply drawing and editing seams on an input model. As demonstrated by our results, our system also supports internal connections, thus significantly broadening the range of shapes that can be designed. Nevertheless, our system has some limitations and many exciting opportunities for future work remain. In particular, input meshes that flatten to exceedingly thin panels pose challenges for subsequent remeshing and optimization. It would be helpful to automatically update the segments connectivity during the optimization and merge thin panels to adjacent panels automatically. Also, we make no attempt at inferring the location of internal connections in an automatic way nor automatically consider geometric properties of our input model such as ridges, symmetries or curvature. Future work could include higher-level tools that exploit this information for supporting the seam placement or for auto-completion of partially drawn seams. Although we have not observed collisions or self-intersecting panels during optimization, we currently do not explicitly prevent these cases. Finally, even with internal connections, there is a limit on what kind of shapes can be obtained with an inflatable structure. For example, planar regions and sharp convex edges (as shown in the "Twisty" example, Figure **??**) are inherently difficult to reproduce. For future work, it would be interesting to indicate at the beginning of the design process infeasible regions and limits on achievable approximations.

Acknowledgements

We would like to thank the reviewers for their insightful comments and Robert Kohn for introducing us to the tension field theory. We also greatly appreciated the help of Urs Meier Aegler, Christian Schumacher and Maurizio Nitti. This work was partly funded by the NCCR Co-Me of the Swiss NSF.

References

BARGTEIL, A. W., WOJTAN, C., HODGINS, J. K., AND TURK, G. 2007. A finite element method for animating large viscoplastic flow. *ACM Trans. Graph. 26*, 3 (July).

BERTHOUZOZ, F., GARG, A., KAUFMAN, D. M., GRINSPUN, E., AND AGRAWALA, M. 2013. Parsing sewing patterns into 3d garments. *Proc. of ACM SIGGRAPH '13*.

BICKEL, B., KAUFMANN, P., SKOURAS, M., THOMASZEWSKI, B., BRADLEY, D., BEELER, T., JACKSON, P., MARSCHNER, S., MATUSIK, W., AND GROSS, M. 2012. Physical face cloning. In *Proc. of ACM SIGGRAPH '12*.

BROUET, R., SHEFFER, A., BOISSIEUX, L., AND CANI, M.-P. 2012. Design preserving garment transfer. *ACM Trans. Graph. 31*, 4 (July), 36:1–36:11.

CHOI, K.-J., AND KO, H.-S. 2002. Stable but responsive cloth. *ACM Trans. Graph. 21*, 3 (July), 604–611.

COROS, S., THOMASZEWSKI, B., NORIS, G., SUEDA, S., FORBERG, M., SUMNER, R. W., MATUSIK, W., AND BICKEL, B. 2013. Computational design of mechanical characters. *ACM Trans. Graph. 32*, 4 (July), 83:1–83:12.

Model	#Elements	#Panels total	#Panels internal	#Remeshing steps	#Iterations / Time [s] preview		#Iterations / Time [s] full convergence	
Sphere	692	3	0	5	8	4	128	21
Teddy	2974	17	0	2	23	17	193	258
Fox	7544	22	3	4	11	35	398	420
Twisty	6084	34	3	2	15	33	247	430
Flower (bottom)	6069	12	1	3	51	60	298	546
Flower (top)	7888	23	0	3	47	69	197	506
Tentacle	4458	21	0	2	9	23	175	131
Elephant	14436	40	2	3	30	137	401	1768

Table 1: *Statistics and processing time for our results. Timings are given for preview quality (relative error between displayed mesh and final result $< 5\%$ of the size of the model) and full convergence (gradient of objective $< 1.e^{-3}$ and forces $< 1.e^{-5}$)*

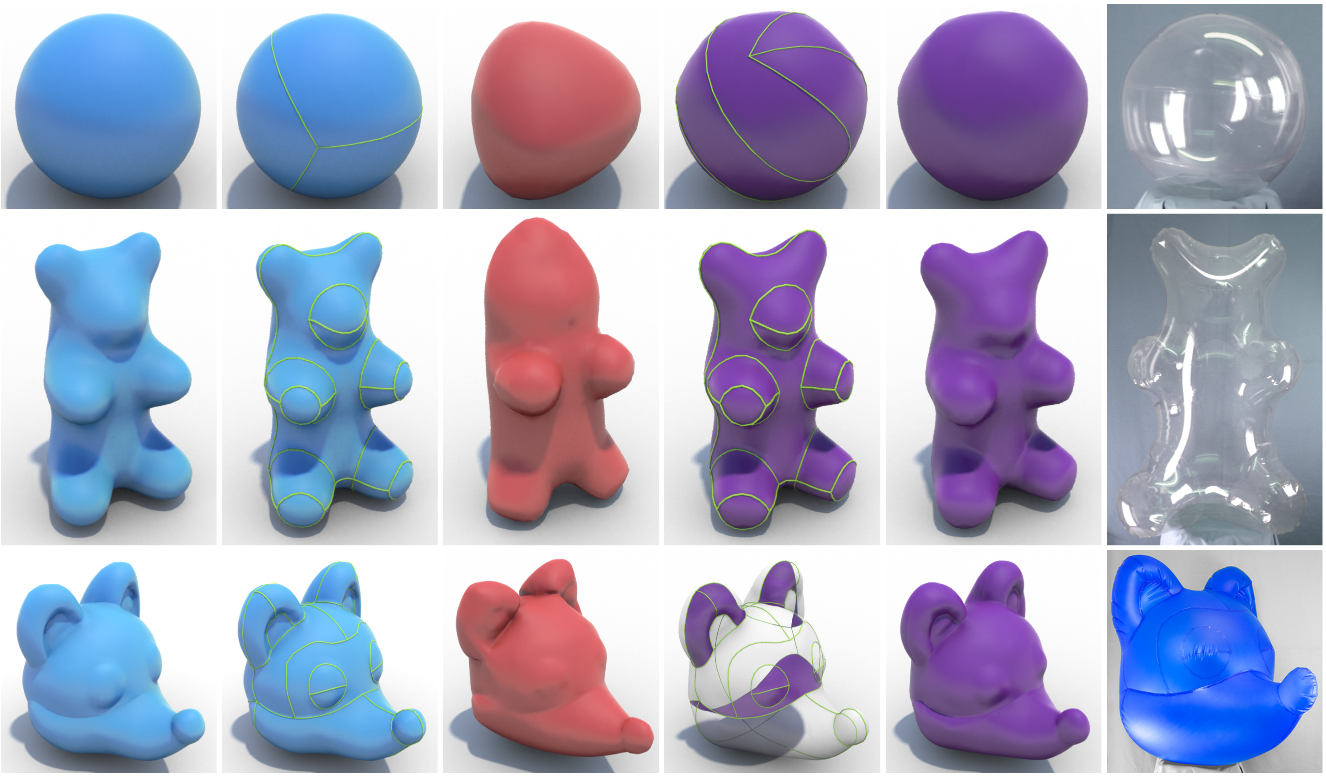

Figure 8: *Overview of our results (from left to right): input model, input model with seam layout, nonoptimized inflated shape, optimized result with seams, optimized result, fabricated prototype. The rows show (from top to bottom) the Sphere, Teddy, and Fox examples.*

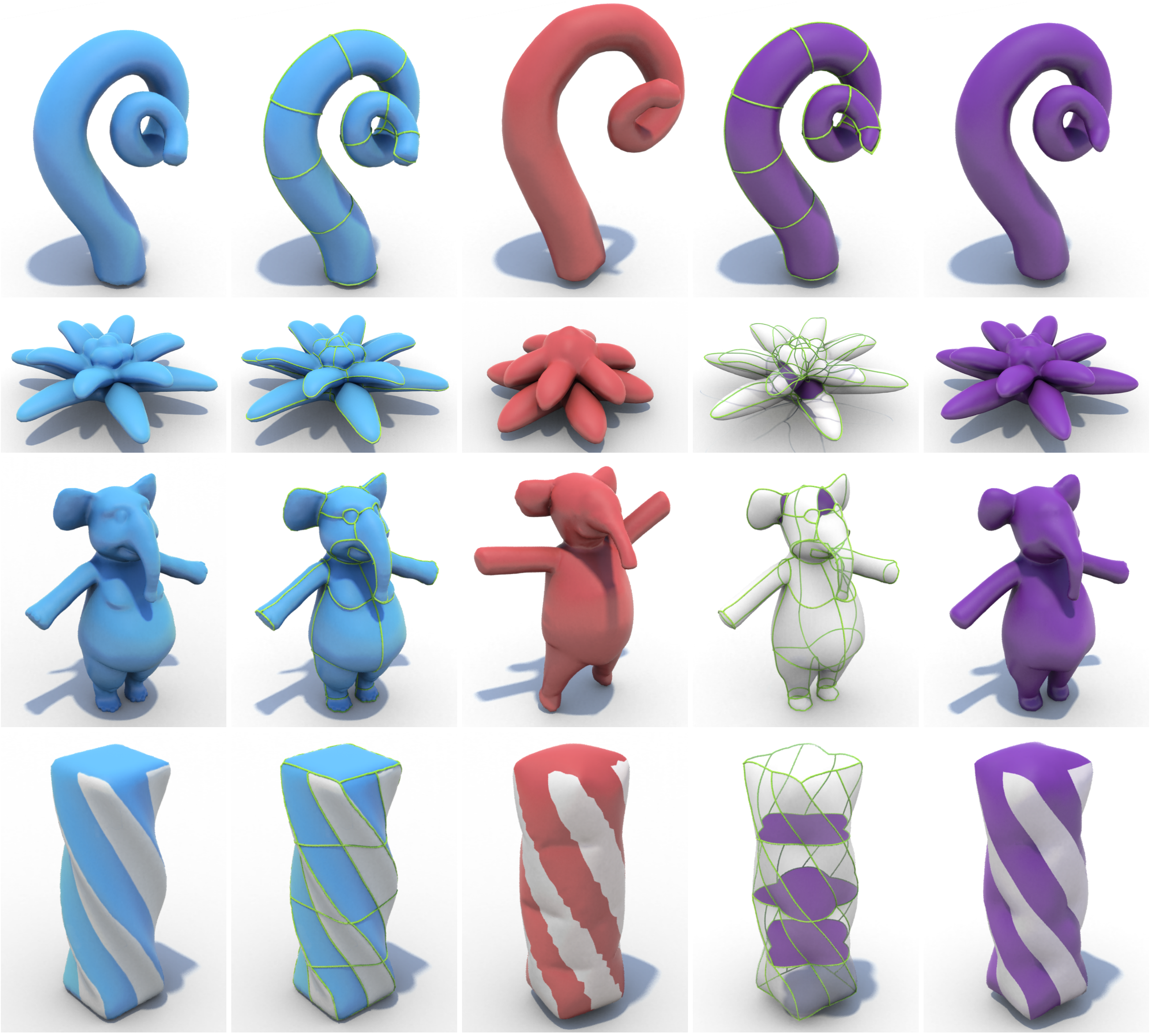

Figure 9: *Overview of results (from left to right): input model, input model with seam layout, nonoptimized inflated shape, optimized result with seams, optimized result without seams. The rows show (from top to bottom) the Tentacle, Flower, Elephant, and Twisty examples.*

FURUTA, Y., UMETANI, N., MITANI, J., IGARASHI, T., AND FUKUI, Y. 2010. A film balloon design system integrated with shell element simulation. *Proc. of EUROGRAPHICS 2010*.

HORMANN, K., LÉVY, B., AND SHEFFER, A. 2007. *Mesh Parameterization: Theory and Practice*. No. 2 in SIGGRAPH 2007 Course Notes. ACM Press, Aug.

JULIUS, D., KRAEVOY, V., AND SHEFFER, A. 2005. D-charts: Quasi-developablemesh segmentation. *Comput. Graph. Forum 24*, 3, 581–590.

KILIAN, M., FLÖRY, S., CHEN, Z., MITRA, N. J., SHEFFER, A., AND POTTMANN, H. 2008. Curved folding. *ACM Trans. Graph. 27*, 3 (Aug.), 75:1–75:9.

LAU, M., OHGAWARA, A., MITANI, J., AND IGARASHI, T. 2011. Converting 3d furniture models to fabricatable parts and connectors. Proc. of ACM SIGGRAPH Asia '11, 85:1–85:6.

MASSARWI, F., GOTSMAN, C., AND ELBER, G. 2007. Papercraft models using generalized cylinders. In *Proc. of Pacific Graphics0́7*, IEEE, 148–157.

MITANI, J., AND SUZUKI, H. 2004. Making papercraft toys from meshes using strip-based approximate unfolding. Proc. of ACM SIGGRAPH '04, 259–263.

MORI, Y., AND IGARASHI, T. 2007. Plushie: An interactive design system for plush toys. *Proc. of ACM SIGGRAPH '07*.

NARAIN, R., SAMII, A., AND O'BRIEN, J. F. 2012. Adaptive anisotropic remeshing for cloth simulation. In *Proc. of ACM SIGGRAPH Asia '12*.

O'BRIEN, J. F., AND HODGINS, J. K. 1999. Graphical modeling and animation of brittle fracture. In *Proceedings of the 26th Annual Conference on Computer Graphics and Interactive Techniques*, SIGGRAPH '99, 137–146.

ROHMER, D., POPA, T., CANI, M.-P., HAHMANN, S., AND SHEFFER, A. 2010. Animation wrinkling: Augmenting coarse cloth simulations with realistic-looking wrinkles. In *ACM SIGGRAPH Asia 2010 Papers*, SIGGRAPH ASIA '10, 157:1–157:8.

SHATZ, I., TAL, A., AND LEIFMAN, G. 2006. Paper craft models from meshes. *The Visual Computer 22*, 9-11, 825–834.

SHEFFER, A., LÉVY, B., MOGILNITSKY, M., AND BOGOMYAKOV, A. 2005. Abf++: Fast and robust angle based flattening. *ACM Trans. Graph. 24*, 2 (Apr.), 311–330.

SKOURAS, M., THOMASZEWSKI, B., BICKEL, B., AND GROSS, M. 2012. Computational design of rubber balloons. In *Proc. of Eurographics '12*.

SKOURAS, M., THOMASZEWSKI, B., COROS, S., BICKEL, B., AND GROSS, M. 2013. Computational design of actuated deformable characters. *ACM Trans. Graph. 32*, 4 (July), 82:1–82:10.

SOLOMON, J., VOUGA, E., WARDETZKY, M., AND GRINSPUN, E. 2012. Flexible developable surfaces. *Comput. Graph. Forum 31*, 5, 1567–1576.

SONG, P., FU, C.-W., GOSWAMI, P., ZHENG, J., MITRA, N. J., AND COHEN-OR, D. 2013. Reciprocal frame structures made easy. 94:1–94:13.

STAVA, O., VANEK, J., BENES, B., CARR, N., AND MĚCH, R. 2012. Stress relief: improving structural strength of 3d printable objects. In *Proc. of ACM SIGGRAPH '12*.

TERAN, J., SIFAKIS, E., IRVING, G., AND FEDKIW, R. 2005. Robust quasistatic finite elements and flesh simulation. In *Proceedings of the 2005 ACM SIGGRAPH/Eurographics Symposium on Computer Animation*, SCA '05, 181–190.

UMETANI, N., KAUFMAN, D. M., IGARASHI, T., AND GRINSPUN, E. 2011. Sensitive couture for interactive garment modeling and editing. In *ACM SIGGRAPH 2011 Papers*, ACM, New York, NY, USA, SIGGRAPH '11, 90:1–90:12.

UMETANI, N., IGARASHI, T., AND MITRA, N. J. 2012. Guided exploration of physically valid shapes for furniture design. *Proc. of ACM SIGGRAPH '12*.

VOUGA, E., HÖBINGER, M., WALLNER, J., AND POTTMANN, H. 2012. Design of self-supporting surfaces. *ACM Trans. Graph. 31*, 4 (July), 87:1–87:11.

WANG, C. 2008. Computing length-preserved free boundary for quasi-developable mesh segmentation. *IEEE Transactions on Visualization and Computer Graphics 14*, 1 (Jan.), 25–36.

WICKE, M., RITCHIE, D., KLINGNER, B. M., BURKE, S., SHEWCHUK, J. R., AND O'BRIEN, J. F. 2010. Dynamic local remeshing for elastoplastic simulation. *ACM Trans. Graph. 29*, 4 (July), 49:1–49:11.

WOJTAN, C., AND TURK, G. 2008. Fast viscoelastic behavior with thin features. *ACM Trans. Graph. 27*, 3 (Aug.), 47:1–47:8.